Preconditioning Methods for Low-Speed Flows

E. Turkel [†] *
V. N. Vatsa [††]
R. Radespiel [†††]

[†] School of Mathematical Sciences
Tel-Aviv University
Tel-Aviv, Israel
and
ICASE, NASA Langley Research Center

[††] NASA Langley Research Center
Hampton, VA

[†††] DLR, Braunschweig
Germany

Abstract

We consider the steady-state equations for a compressible fluid. For low-speed flow, the system is stiff because the ratio of the convective speed to the speed of sound is quite small. To overcome this difficulty, we alter the time evolution of the equations but retain the same steady-state analytic equations. To achieve high numerical resolution, we also alter the artificial viscosity of the numerical scheme, which is implemented conveniently by using other sets of variables in addition to the conservative variables. We investigate the effect of the artificial dissipation within this preconditioned system. We consider both the nonconservative and conservative formulations for artificial viscosity and examine their effect on the accuracy and convergence of the numerical solutions. The numerical results for viscous three-dimensional wing flows and two-dimensional multi-element airfoil flows indicate that efficient multigrid computations of flows with arbitrarily low Mach numbers are now possible with only minor modifications to existing compressible Navier-Stokes codes. The conservative formulation for artificial viscosity, coupled with the preconditioning, offers a viable computational fluid dynamics (CFD) tool for analyzing problems that contain both incompressible and compressible flow regimes.

*This research was supported in part by the National Aeronautics and Space Administration under NASA Contract No. NAS1-19480 while the first author was in residence at the Institute for Computer Applications in Science and Engineering (ICASE), NASA Langley Research Center, Hampton, VA 23681-0001.

1 Introduction

In the past few years, several preconditioning methods have appeared in the literature [1-4] with the aim of solving nearly incompressible flow problems with numerical algorithms that were designed for compressible flows. The development of these methods are motivated by two main observations. First, flow problems exist that contain both compressible and incompressible flows simultaneously; that is, part of the flow region can be considered to be incompressible with locally low Mach numbers, whereas significant compressibility effects occur in other regions of the flow. A typical example in aerodynamics is the flow over a multielement airfoil near maximum lift. Surface heat transfer or volumetric heat addition can also introduce compressibility effects in low-speed flows. Second, it is preferable to use existing compressible flow codes over the broadest range of flow conditions possible for ease of use and consistency reasons.

The difficulty in solving the compressible equations for low Mach numbers is attributed to the large disparity of the acoustic wave speed, $u+a$, and the waves convected at the fluid speed, u. The application of preconditioning changes the eigenvalues of the system of compressible flow equations and reduces this disparity in the wave speeds. For example, the time derivatives are premultiplied by a matrix that slows the speed of the acoustic waves relative to the fluid speed.

The preconditionings that are applied here not only accelerate the convergence to a steady state but can also change the steady-state solution because of the choice of artificial viscosity, or upwinding, terms. Similarly, the boundary conditions are based on the preconditioned equations rather than the original governing equations. As discussed in ref. [9], the "standard" numerical schemes for the compressible equations do not converge to the solution of the incompressible equations (using a pseudo-compressibility approach) as the Mach number approaches zero. However, the use of a proper preconditioning leads to a numerical scheme that does behave appropriately for low Mach numbers.

In this paper, we present a generalization of the preconditioners given by Turkel [10]- [11], and Choi and Merkle [1], as well as those presented more recently by Radespiel and Turkel [6] and Radespiel et al. [7]. We discuss both nonconservative and conservative artificial dissipation models and the effects of the preconditioning matrix on the accuracy. Numerical results indicate that by using the conservative formulation of artificial dissipation model, accurate solutions are obtained without sacrificing efficiency.

We show that preconditioning can be combined with well-known convergence acceleration techniques such as residual smoothing and multigrid. Indeed, the clustering of eigenvalues with preconditioning improves the damping of transient high-frequency modes to an extent, which makes efficient multigrid computation of low Mach number flows practical.

Algorithm

The conservation-law form of the Euler equations can be transformed easily into non-conservation form by matrix transformations and vice-versa. For convenience, we start with the non-conservation form of the Euler equations. Note that although the theory is developed for the Euler equations, the methodology is applied in a straight-forward manner to the Navier-Stokes equations by grouping the viscous fluxes with the dissipative fluxes.

We consider the preconditioned Euler equations written as

$$P^{-1}Q_t + AQ_x + BQ_y + CQ_z = 0 \tag{1}$$

The form of the matrices A, B, and C depends on the choice of variables Q. We first consider the variables $Q = Q_0 = (p, u, v, w, S)$, where the entropy satisfies the relation $dS = dp - a^2 d\rho$. We then have the following form of the matrices for Q_0:

$$A_0 = \begin{pmatrix} u & \rho a^2 & 0 & 0 & 0 \\ \frac{1}{\rho} & u & 0 & 0 & 0 \\ 0 & 0 & u & 0 & 0 \\ 0 & 0 & 0 & u & 0 \\ 0 & 0 & 0 & 0 & u \end{pmatrix}, B_0 = \begin{pmatrix} v & 0 & \rho a^2 & 0 & 0 \\ 0 & v & 0 & 0 & 0 \\ \frac{1}{\rho} & 0 & v & 0 & 0 \\ 0 & 0 & 0 & v & 0 \\ 0 & 0 & 0 & 0 & v \end{pmatrix}, \mathrm{C}_0 = \begin{pmatrix} w & 0 & 0 & \rho a^2 & 0 \\ 0 & w & 0 & 0 & 0 \\ 0 & 0 & w & 0 & 0 \\ \frac{1}{\rho} & 0 & 0 & w & 0 \\ 0 & 0 & 0 & 0 & w \end{pmatrix}$$

In generalized coordinates, we are interested in combinations of these matrices. Hence, we define $D_0 = A_0\omega_1 + B_0\omega_2 + C_0\omega_3$ and $q = u\omega_1 + v\omega_2 + w\omega_3$, where ω_1, ω_2, and ω_3 are the metrics associated with the coordinate transformation. This definition leads to

$$D_0 = \begin{pmatrix} q & \rho a^2\omega_1 & \rho a^2\omega_2 & \rho a^2\omega_3 & 0 \\ \frac{1}{\rho}\omega_1 & q & 0 & 0 & 0 \\ \frac{1}{\rho}\omega_2 & 0 & q & 0 & 0 \\ \frac{1}{\rho}\omega_3 & 0 & 0 & q & 0 \\ 0 & 0 & 0 & 0 & q \end{pmatrix}$$

We consider the preconditioner P_0 given by

$$P_0^{-1} = \begin{pmatrix} \frac{a^2}{\beta^2} & 0 & 0 & 0 & \delta \\ \frac{\alpha u}{\rho\beta^2} & 1 & 0 & 0 & 0 \\ \frac{\alpha v}{\rho\beta^2} & 0 & 1 & 0 & 0 \\ \frac{\alpha w}{\rho\beta^2} & 0 & 0 & 1 & 0 \\ 0 & 0 & 0 & 0 & 1 \end{pmatrix}, \qquad P_0 = \begin{pmatrix} \frac{\beta^2}{a^2} & 0 & 0 & 0 & -\frac{\beta^2}{a^2}\delta \\ -\frac{\alpha u}{\rho a^2} & 1 & 0 & 0 & \frac{\alpha u}{\rho a^2}\delta \\ -\frac{\alpha v}{\rho a^2} & 0 & 1 & 0 & \frac{\alpha v}{\rho a^2}\delta \\ -\frac{\alpha w}{\rho a^2} & 0 & 0 & 1 & \frac{\alpha w}{\rho a^2}\delta \\ 0 & 0 & 0 & 0 & 1 \end{pmatrix} \tag{2}$$

where α, β, and δ are free parameters.

For optimal preconditioning, β^2 should be proportional to the square of the local speed, $u^2 + v^2 + w^2$, ([11]). However, this strategy introduces a complication near the stagnation points; the preconditioner becomes singular when $\beta = 0$. Furthermore, Darmofal and Schmid [3] have shown that the eigenvectors become less orthogonal as β goes to zero. We introduce a simple cutoff to avoid this situation. Because this preconditioner is introduced mainly for low-speed regions, we design the preconditioner to turn off at higher speeds. If the preconditioner is turned off at a subsonic Mach number we can use a nonconservative formulation for the artificial viscosity without a loss of accuracy in capturing weak solutions. As shown later, this strategy simplifies the construction of an artificial viscosity. For sufficiently high Mach numbers, we want to remove the preconditioning, i.e. $\beta^2 = a^2$, $\alpha = 0$, and $\delta = 0$. One choice is

$$\beta^2 = \min\left[\max\left(K_1(u^2 + v^2 + w^2)(1 + \frac{1 - M_0^2}{M_0^4}M^2), K_2^2(u_\infty^2 + v_\infty^2 + w_\infty^2)\right),\ a^2\right] \tag{3}$$

For nonorthogonal grids, $u^2 + v^2 + w^2$ can be replaced by the sum of the squares of the normalized contravariant velocity components.

The case of no preconditioning ($P = I$) corresponds to $\alpha = 0, \beta^2 = a^2$, and $\delta = 0$. The parameter β^2 is returned to its nonpreconditioned value at M_0, which is the cutoff value for the

Mach number. Numerical evidence suggests that K_2 depends on the number of mesh nodes near the stagnation point and possibly should depend on the local cell Reynolds number [1]. Typically, K_1 is between 1 and 1.1, and K_2 is between 0.4 and 1. The eigenvalues of the matrix $P_0 D_0$ are

$$\lambda_0 = q, q, q \quad \text{(repeated eigenvalues)}$$

and

$$\lambda_\pm = \left(zq \pm \sqrt{z^2 q^2 + \beta^2 (|\omega|^2 - \frac{q^2}{a^2})} \right), \qquad z = 0.5(1 - \alpha + \frac{\beta^2}{a^2}). \tag{4}$$

So $\Lambda = diag(\lambda_+, \lambda_-, \lambda_0, \lambda_0, \lambda_0)$.

The eigenvalues of $P_0 D_0$ are independent of δ; however, the same is not true for the eigenvectors. Though Choi and Merkle [1] employ $\delta = 1$, we consider $\delta = 0$ because this simplifies the eigenvectors of $P_0 D_0$. The right eigenvectors are given by the columns of

$$R^{-1} = \begin{pmatrix} \rho\beta^2 & \rho\beta^2 & 0 & 0 & 0 \\ \frac{\beta^2\omega_1 - \alpha u \lambda_+}{\lambda_+ - q} & \frac{\beta^2\omega_1 - \alpha u \lambda_-}{\lambda_- - q} & -\omega_2 & 0 & 0 \\ \frac{\beta^2\omega_2 - \alpha v \lambda_+}{\lambda_+ - q} & \frac{\beta^2\omega_2 - \alpha v \lambda_-}{\lambda_- - q} & \omega_1 & \omega_3 & 0 \\ \frac{\beta^2\omega_3 - \alpha w \lambda_+}{\lambda_+ - q} & \frac{\beta^2\omega_3 - \alpha w \lambda_-}{\lambda_- - q} & 0 & -\omega_2 & 0 \\ 0 & 0 & 0 & 0 & 1 \end{pmatrix}$$

Note that $(\lambda_+ - q)(\lambda_- - q) = \alpha q^2 - \beta^2 |\omega|^2$. We define some temporary quantities. Let

$$\begin{aligned}
r_{31} &= \frac{\alpha(u|\omega|^2 - q\omega_1)}{\rho\omega_2(\lambda_+ - q)(\lambda_- - q)} \\
r_{32} &= \frac{-1}{\omega_2} - \frac{\omega_1(\beta^2\omega_1 - \alpha u q)}{\omega_2(\lambda_+ - q)(\lambda_- - q)} \\
r_{33} &= \frac{-(\beta^2\omega_1 - \alpha u q)}{(\lambda_+ - q)(\lambda_- - q)} \\
r_{34} &= \frac{-\omega_3(\beta^2\omega_1 - \alpha u q)}{\omega_2(\lambda_+ - q)(\lambda_- - q)} \\
r_{41} &= \frac{\alpha(w|\omega|^2 - q\omega_3)}{\rho\omega_2(\lambda_+ - q)(\lambda_- - q)} \\
r_{42} &= \frac{-\omega_1(\beta^2\omega_3 - \alpha w q)}{\omega_2(\lambda_+ - q)(\lambda_- - q)} \\
r_{43} &= \frac{-(\beta^2\omega_3 - \alpha w q)}{(\lambda_+ - q)(\lambda_- - q)} \\
r_{44} &= \frac{-1}{\omega_2} - \frac{\omega_3(\beta^2\omega_3 - \alpha w q)}{\omega_2(\lambda_+ - q)(\lambda_- - q)}
\end{aligned}$$

Then

$$R = \begin{pmatrix} \frac{\lambda_+ - (1-\alpha)q}{\rho\beta^2(\lambda_+ - \lambda_-)} & \frac{\omega_1}{\lambda_+ - \lambda_-} & \frac{\omega_2}{\lambda_+ - \lambda_-} & \frac{\omega_3}{\lambda_+ - \lambda_-} & 0 \\ -\frac{\lambda_- - (1-\alpha)q}{\rho\beta^2(\lambda_+ - \lambda_-)} & \frac{-\omega_1}{\lambda_+ - \lambda_-} & \frac{-\omega_2}{\lambda_+ - \lambda_-} & \frac{-\omega_3}{\lambda_+ - \lambda_-} & 0 \\ r_{31} & r_{32} & r_{33} & r_{34} & 0 \\ r_{41} & r_{42} & r_{43} & r_{44} & 0 \\ 0 & 0 & 0 & 0 & 1 \end{pmatrix} \tag{5}$$

Note that R is singular for $\omega_2 = 0$, which is merely an artifact because multiple eigenvalues exist in a multidimensional eigenspace. If $\omega_2 = 0$, then we can change the eigenvectors in the invariant subspace of the multiple eigenvalues so that either ω_1 or ω_3 appears in the denominator. Because all three of these eigenvalues cannot be zero simultaneously, some set of nonsingular eigenvectors always exists. Also note that ω_2 does not appear in the denominator in the final analysis and does not create any numerical difficulties; therefore we can ignore this anomaly.

The largest eigenvalue of $P_0 D_0$ is used to determine the (inviscid) time step. For $M \sim 0$, $\lambda_\pm \sim 0.5q\left((1-\alpha) \pm \sqrt{(1-\alpha)^2+4}\right)$. For $\alpha = 0$, the condition number of $P_0 D_0$ is $\frac{1+\sqrt{5}}{1-\sqrt{5}} \sim 2.6$, and for $\alpha = 1$ the condition number is 1.

The above matrices were given for $Q_0 = (p, u, v, w, S)$ variables. In the code we base everything on $Q_4 = (p, u, v, w, T)$ variables. Then,

$$P_4 = \frac{\partial Q_4}{\partial Q_0} P_0 \frac{\partial Q_0}{\partial Q_4}$$

The transformations between the Q_0 and Q_4 variables are given in the appendix.

Artificial Viscosity

For a central-difference scheme, it is necessary to add artificial dissipative terms to the finite-difference approximation of the spatial derivatives to damp the numerical oscillations. A nonlinear second-difference term is normally added to control oscillations near shocks, and a linear fourth-difference term is added to damp high-frequency oscillations [5]. We are interested primarily in the functional form of these differences. Hence, our examples include a second-difference artificial dissipation; extensions to fourth differences and nonlinearities are straight-forward. Similarly, for one-sided schemes the central difference plus the artificial dissipation is replaced by a Roe matrix formulation.

A typical preconditioned finite-difference scheme can be expressed as

$$\Delta Q_c = \Delta t P_c \left[\frac{\partial F}{\partial x} + \frac{\partial G}{\partial y} + \frac{\partial H}{\partial z}\right] = \Delta t P_c \left[A_c \frac{\partial Q_c}{\partial x} + B_c \frac{\partial Q_c}{\partial y} + C_c \frac{\partial Q_c}{\partial z}\right] \tag{6}$$

where Q_c represents the conservative variables and the spatial partial derivatives are replaced by central-difference approximations. We consider both conservative and non-conservative ways of adding artificial dissipative terms. The dissipation need not be expressed in terms of the conservative variables Q_c. For another set of variables Q_V, we get $\Delta Q_c = \frac{\partial Q_c}{\partial Q_V} \Delta Q_V$. We choose our "basic" form as the one given in $Q_0 = (p, u, v, w, S)$ variables (i.e., P_0). Then, for another set of variables Q_V, we have the preconditioner $\Gamma_V = \frac{\partial Q_V}{\partial Q_c} P_c = P_V \frac{\partial Q_V}{\partial Q_c} = \frac{\partial Q_V}{\partial Q_0} P_0 \frac{\partial Q_0}{\partial Q_c}$.

We add second-difference terms for the artificial viscosity to Eq. (6) and omit the fourth differences for brevity. We now get

$$\begin{aligned} \Delta Q_V &= \Delta t \left\{ \Gamma_V \left[\frac{\partial F}{\partial x} + \frac{\partial G}{\partial y} + \frac{\partial H}{\partial z}\right] \right. \\ &+ \left. \left(|\sigma(P_V A_V)| \frac{\partial Q_V}{\partial x}\right)_x + \left(|\sigma(P_V B_V)| \frac{\partial Q_V}{\partial y}\right)_y + \left(|\sigma(P_V C_V)| \frac{\partial Q_V}{\partial z}\right)_z \right\} \end{aligned} \tag{7}$$

where $\Gamma_V = P_V \frac{\partial Q_V}{\partial Q_c}$. Thus, Γ_V contains both the preconditioner and the change of variables. The above formulation is non-conservative because Γ_V is outside the derivative terms. In the above

equation, σ is a matrix function. For example, if σ is proportional to the spectral radius, then we have a scalar artificial viscosity in Q_V variables; whereas if $\sigma(A) \sim A$, then we have a matrix-valued artificial viscosity.

After we have computed ΔQ_V, we perform the residual smoothing on it. In the multigrid algorithm, ΔQ_V is passed to the next coarser grid. At the end of each stage, Q_V is recomputed. The conservative variables are then calculated as nonlinear functions of the Q_V variables. We should mention that $A_V = \frac{\partial Q_V}{\partial Q_c} A_c \frac{\partial Q_c}{\partial Q_V}$; similar expressions can be written for the other coordinate directions. Let $\hat{A_V} = \frac{\partial F}{\partial Q_V}$ be the Jacobian matrix; then, $\hat{A_V} = \frac{\partial Q_c}{\partial Q_V} A_V$. Hence,

$$P_V A_V = \frac{\partial Q_V}{\partial Q_c} P_c A_c \frac{\partial Q_c}{\partial Q_V} = \Gamma_V A_c \frac{\partial Q_c}{\partial Q_V}$$

Because the spectral radius is invariant under a similarity transformation for a scalar viscosity, we can use either $P_V A_V$ or $P_c A_c$. Let $\Lambda = \mathrm{diag}(\lambda_1, \lambda_2, \lambda_3, \lambda_3, \lambda_3)$, where λ_1, λ_2, and λ_3 represent λ_+, λ_-, and λ_0 (i.e., the eigenvalues of PD), modified by cutoffs near the stagnation points. Define $|\Lambda| = \mathrm{diag}(|\lambda_1|, |\lambda_2|, |\lambda_3|, |\lambda_3|, |\lambda_3|)$. Then, $|PD| = R^{-1}|\Lambda|R$. For any vector $x = (x_1, x_2, x_3, x_4, x_5)^t$, $|PD|x = (R^{-1}|\Lambda|)z$, where $z = Rx$. Define $Y = \omega_1 x_2 + \omega_2 x_3 + \omega_3 x_4$. Then,

$$z = \begin{pmatrix} \frac{1}{\lambda_+ - \lambda_-}\left[\frac{\lambda_+ - (1-\alpha)q}{\rho\beta^2} x_1 + Y\right] \\ -z_1 + \frac{x_1}{\rho\beta^2} \\ z_3 \\ z_4 \\ (1-\gamma)x_1 + \frac{\gamma p}{T} x_5 \end{pmatrix}$$

where z_1 is the first element of the vector z. We note that z_3 and z_4 do not appear by themselves in subsequent formulas but rather in conjunction with other variables in the form

$$\begin{aligned} \omega_2 z_3 &= -x_2 + \frac{1}{(\lambda_+ - q)(\lambda_- - q)}\left[\frac{\alpha(u|\omega|^2 - q\omega_1)}{\rho} x_1 - (\beta^2\omega_1 - \alpha u q)Y\right] \\ \omega_2 z_4 &= -x_4 + \frac{1}{(\lambda_+ - q)(\lambda_- - q)}\left[\frac{\alpha(w|\omega|^2 - q\omega_3)}{\rho} x_1 - (\beta^2\omega_3 - \alpha w q)Y\right] \\ \omega_1 z_3 + \omega_3 z_4 &= x_3 - \frac{1}{(\lambda_+ - q)(\lambda_- - q)}\left[\frac{\alpha(v|\omega|^2 - q\omega_2)}{\rho} x_1 - (\beta^2\omega_2 - \alpha v q)Y\right] \end{aligned}$$

So

$$|PD|x = R^{-1}|\Lambda|z = \begin{pmatrix} \rho\beta^2(|\lambda_1|z_1 + |\lambda_2|z_2) \\ \frac{\beta^2\omega_1 - \alpha u\lambda_+}{\lambda_+ - q}|\lambda_1|z_1 + \frac{\beta^2\omega_1 - \alpha u\lambda_-}{\lambda_- - q}|\lambda_2|z_2 - (\omega_2 z_3)|\lambda_3| \\ \frac{\beta^2\omega_2 - \alpha v\lambda_+}{\lambda_+ - q}|\lambda_1|z_1 + \frac{\beta^2\omega_2 - \alpha v\lambda_-}{\lambda_- - q}|\lambda_2|z_2 + (\omega_1 z_3 + \omega_3 z_4)|\lambda_3| \\ \frac{\beta^2\omega_3 - \alpha w\lambda_+}{\lambda_+ - q}|\lambda_1|z_1 + \frac{\beta^2\omega_3 - \alpha w\lambda_-}{\lambda_- - q}|\lambda_2|z_2 - (\omega_2 z_4)|\lambda_3| \\ \frac{T}{\gamma p}\left[(\gamma - 1)|\lambda_1|z_1 + |\lambda_3|z_5\right] \end{pmatrix}.$$

For a scalar viscosity (i.e., when σ is the spectral radius), the viscosity remains scalar after preconditioning. In this approach, differences of the Q_V variables, rather than those of the conserved variables, are added to each of the conservation equations.

However, the formulation used until now is nonconservative. Since we are also interested in solving transonic flows with shocks using this scheme, we present a conservative formulation of the artificial dissipation. By dropping the subscript V, we obtain

$$\Delta Q = \Delta t \Gamma \left\{ \frac{\partial F}{\partial x} + \frac{\partial G}{\partial y} + \frac{\partial H}{\partial z} + \left(\Gamma^{-1} |\sigma(PA)| \frac{\partial Q}{\partial x} \right)_x + \left(\Gamma^{-1} |\sigma(PB)| \frac{\partial Q}{\partial y} \right)_y + \left(\Gamma^{-1} |\sigma(PC)| \frac{\partial Q}{\partial z} \right)_z \right\}$$

Even if σ is a scalar function, we must evaluate a matrix-vector product; as a result, the numerical effort is equivalent in complexity to a matrix-valued viscosity.

Following previous work on multigrid schemes for the Navier-Stokes equations, these artificial viscosity functions account for the ratio of the spectral radii in the different coordinate directions; that is,

$$\sigma(PA) = k^{(4)} \tilde{\sigma}(PA) \left[1 + \left(\frac{\rho(PB)}{\rho(PA)} \right)^{\zeta} + \left(\frac{\rho(PC)}{\rho(PA)} \right)^{\zeta} \right]$$

where $\tilde{\sigma}$ denotes the original viscosity function, ρ denotes the spectral radius, and $k^{(4)}$ is the artificial viscosity coefficient that corresponds to the fourth-difference terms. Similar relations are used to modify the artificial viscosity by cell aspect-ratio in the other coordinate directions. These scaling functions provide sufficient artificial dissipation for general curvilinear grids that contain high aspect-ratio cells.

In the previous section, a preconditioner was introduced that is dependent on the parameters α and δ. Because δ does not affect the eigenvalues of PA, it has no affect on the scalar artificial viscosity. Choosing $\alpha = 1$ reduces the largest eigenvalue, which also improves the condition number and decreases the artificial viscosity compared with $\alpha = 0$ case. We thus expect $\alpha = 1$ to slow the convergence compared with the case in which $\alpha = 0$, in spite of the fact that we have reduced the condition number. However, we expect that with $\alpha = 1$, the numerical accuracy will improve. For a matrix viscosity (or a Roe matrix), we expect similar but less pronounced dependence on α.

Boundary Conditions

In many CFD codes, the boundary conditions in the far field are based on characteristic variables, even for viscous flow. Thus, at inflow the incoming variables that correspond to positive eigenvalues are specified, and the outgoing variables that correspond to negative eigenvalues are extrapolated. A change in the time-dependent equations also changes the characteristics of the system (although the signs of the eigenvalues remain unchanged). Hence, the boundary conditions must be modified for the preconditioned system.

In the present study, we have used the simplified far-field boundary conditions suggested in ref. [6]. Basically, all variables at far-field boundaries are specified in terms of two sets for p, u, v, w, and T. Depending on whether the subsonic flow is an inflow or an outflow, one set is specified at the free-stream levels, and the other set is extrapolated from the interior. For example, at the inflow

$$u_b = u_\infty, v_b = v_\infty, \mathrm{w_b} = \mathrm{w}_\infty, T_b = T_\infty, \mathrm{p_b} = \mathrm{p_{int}}$$

and at the outflow

$$u_b = u_{int}, v_b = v_{int}, \mathrm{w_b} = \mathrm{w_{int}}, T_b = T_{int}, \mathrm{p_b} = \mathrm{p}_\infty$$

where the subscripts "b" and "int" refer to the values at the boundary and adjacent interior points, respectively.

For supersonic flows, standard boundary conditions are used; that is, extrapolation at the outflow boundary and free-stream values for all variables at the inflow boundary are prescribed.

Changes to Original Coding

Here, we present the steps necessary to introduce preconditioning into an existing compressible flow code. We assume an explicit time-stepping scheme (e.g., a Runge-Kutta scheme) that is augmented by an implicit residual smoothing and multigrid scheme to obtain steady-state solutions.

1. Precondition the residual.

   - Select a reasonable set of dependent variables for the problem (e.g., p, u, v, w, T). Note that other sets of variables are possible.
   - For nonconservative scalar artificial viscosity
     - Multiply the physical residual (inviscid and Navier-Stokes portions and physical forcing functions (if applicable)) by $\Gamma = P_T \frac{\partial Q_4}{\partial Q_1}$.
     - Add scalar artificial viscosity in these new variables to the residual.
   - For conservative scalar viscosity
     - Add inviscid, viscous, and artificial viscosity fluxes to obtain the total residual. Scalar viscosity already includes the transformation Γ^{-1}.
     - Multiply this total residual by Γ.
   - Multiply the total preconditioned residual in the (p, u, v, w, T) by Δt. Apply the residual smoothing for the changes in terms of the (p, u, v, w, T) variables. Add the residuals in the (p, u, v, w, T) variables to the dependent variables at the previous time iteration to obtain the values of (p, u, v, w, T) at the next time step. The new values of the conservative variables are then evaluated as nonlinear functions of (p, u, v, w, T).

2. For the FAS multigrid algorithm, we need to restrict the residuals and the variables from a finer grid to a coarser grid. In the computer code, the residuals are stored in the (p, u, v, w, T) frame, whereas the dependent variables are stored as conservative variables. Hence, restrictions and prolongations are done on the conservative variables. The residual smoothing is performed on the (p, u, v, w, T) residuals and the forcing functions on the coarse grids are evaluated in (p, u, v, w, T) variables.

3. Choose a new time step for the inviscid portion based on the preconditioned system. The viscous contribution to the time step is then incorporated as usual.

4. Modify the far-field boundary conditions.

Computational Results

An existing three-dimensional compressible Navier-Stokes flow solver was modified to include the preconditioning methodology described in the preceding paragraphs. The modified code was used

	Mach no.	panel method	no preconditioning	preconditioning
C_L	0.1	.241	.2448	.2434
	0.01		.2172	.2421
	0.001		.1097	.2421
C_D	0.1	0.0	.0008	.00027
	0.01		.0086	.00027
	0.001		.0731	.00027

Table 1: Comparison of lift and drag with/without preconditioning

to compute low-speed and transonic flow over several configurations of practical interest. Three of these test cases are discussed here. The computational results reported in this paper were obtained with scalar form of artificial dissipation.

Two Dimensional Results

We first consider a two dimensional inviscid subsonic problem. For this case we can compare the compressible code with and without preconditioning to a panel method in order to assess their accuracy. We consider inviscid flow over NACA 0012 airfoil. The C-type grid has 224×40 cells clustered near the leading and trailing edges in order to allow accurate drag computations. As seen in table 1 the code using the preconditioning gives lift and drag quite close to the panel method results with only a small dependence on the Mach number. The non-preconditioned code has large variations as the Mach number goes to zero and is not converging to the panel code results. In particular the drag, which should be zero for inviscid flow, is very large without preconditioning but close to zero when using preconditioning.

Low-Speed Flow over Three-Dimensional Wing

Essentially incompressible viscous flow over the ONERA M6 wing is considered as the first test case. For this case, the Reynolds number (based on mean aerodynamic chord) is 11.7 million, and the angle of attack is 3.06°. A grid that consists of $193 \times 49 \times 33$ points is used for these computations.

The first set of results in Fig. 1 shows the effect of preconditioning on the convergence history of the numerical algorithm at a Mach number of 0.1. For these computations, 50 iterations on the coarse grid are followed by 300 iterations on the fine grid. This figure clearly shows a significant improvement in the convergence rate when preconditioning is used.

The effect of the free-stream Mach number is considered in the next series. Figures 2 - 3 show the effect of free-stream Mach number on convergence rates and surface pressure distribution, respectively. The residuals in Fig. 2 have been normalized with their respective initial values to remove the scaling effects caused by differences in the free-stream Mach number. Note that over a Mach number range of 0.01 to 0.2, the convergence rates for the preconditioned scheme are very similar; the asymptotic convergence rates for the two lowest Mach numbers are almost identical. Although not shown here, similar results have been obtained at an even lower Mach number of

0.001. On the other hand, the original non-preconditioned scheme failed to converge at Mach numbers of 0.01 and lower; similar to the observations reported by Volpe [12].

The pressure distributions (at a span location of 80%) shown in Fig. 3 indicate that results for Mach numbers of 0.01 and 0.1 are identical within plotting accuracy. Even at a Mach number of 0.2 (except for a slightly higher value of the pressure peak in the leading-edge region), the effect of Mach number is negligible. These results demonstrate that the preconditioned system approaches the incompressible limit in a smooth and systematic manner without any penalty in convergence rate.

The effects of the conservative and non-conservative form of the artificial viscosity formulations are shown in Figs. 4 and 5. The non-conservative formulation converges better on the coarser grid, but is nearly identical in performance to the conservative formulation on the fine grid. The effect of these two forms of artificial viscosity on pressure distribution is negligible, which is expected to be the case at low speeds.

Flow over Two-Dimensional Multi-element Airfoil

The next test case considered here is that of a 3-element airfoil configuration that has been investigated both experimentally and theoretically [13]. Present computations are performed at a chord Reynolds number of 9 million and an angle of attack of 16.2°. The Mach number for this test case is 0.2. A 20-block structured grid, shown in Fig. 6, is used for the computations. This test case has also been investigated with the original non-preconditioned version of the flow solver used in this work, as reported by Vatsa et al. [14].

The convergence histories for this case are presented in Fig. 7, where the results from the original non-preconditioned and current preconditioned (conservative) schemes are compared. The residuals in the original scheme indicate considerable slowdown in convergence at approximately 4-orders; whereas the residuals in the preconditioned scheme exhibit much better convergence. Note that the free-stream Mach number of 0.2 for this case is not considered too low for compressible codes. However, in this case several pockets of slow-moving flow exist in the cove regions of the slat and the main airfoil sections [14]; these pockets slow the convergence of standard compressible codes. The preconditioned system has a much better condition number for the eigenvalues and does not experience slowdown as a result of such disparities in the flow speed.

The computed pressure distributions for this case are compared in Fig. 8. As expected, little difference is observed in the two sets of computed results; furthermore, these results compare quite favorably with the experimental data.

Transonic Flow over Three-Dimensional Wing

The final test case presented here involves transonic flow over the ONERA M6 wing. The test conditions for this case are identical to the first test case except for the free-stream Mach number, which is chosen as 0.84. The Navier-Stokes solutions for this case were obtained for conservative and non-conservative preconditioners. A baseline solution with no preconditioning was also obtained for comparison.

The computed pressure distributions for this case are compared in Fig. 9 at 80% span station. This figure clearly shows that the pressure distributions from conservative preconditioning are virtually indistinguishable from the baseline (unpreconditioned) case. However, the non-conservative

form of preconditioning produces noticeable differences in the pressure distribution in the vicinity of the shocks.

The convergence histories for this case are shown in Fig. 10, where it is observed that the baseline scheme stalls once the residual drops approximately 4-orders in magnitude. The convergence properties of the two preconditioned schemes are similar to one another and better than those of the baseline scheme. Note that the slow convergence of the basic scheme cannot be attributed to low free-stream velocities. However, the computational domain consists of low-speed flows in the stagnation and boundary-layer regions, where the convective speed of propagation is much slower. Preconditioning appears to reduce the imbalance of convective and acoustic speeds in these regions, which improves the overall convergence rate for such problems.

Concluding Remarks

An attractive scheme for computing low-speed flows has been presented here in the framework of a preconditioning applied to the compressible flow equations. The current formulation produces accurate incompressible results in a smooth and systematic manner as the Mach number approaches zero. Moreover, the proposed scheme is relatively easy to implement in an existing compressible flow code.

The test cases presented here demonstrate the efficiency and accuracy of the preconditioned scheme. Excellent convergence has been obtained at Mach numbers that range from 0.01 to 0.84. The resulting pressure distributions agree well with known solutions for these cases. Based on our experience thus far, this scheme offers a viable alternative to purely incompressible flow codes for computing low-speed flows. In addition, this scheme offers the advantage of being able to compute flows with mixed speed regimes, in which the local Mach numbers can vary from very low subsonic to supersonic values, e.g., in the case of flow over high-lift configuration near maximum lift. Finally, this scheme can improve the convergence rate even for viscous transonic flows by preconditioning the embedded low-speed flows in the boundary layers. Future work should focus on matrix-dissipation or Roe type schemes, to improve the numerical accuracy.

Appendix

We define the sets of variables

$$Q_0 = (p, u, v, w, S)$$

$$Q_c = Q_1 = (\rho, \rho u, \rho v, \rho w, E)$$

and

$$Q_4 = (p, u, v, w, T).$$

Let a be the speed of sound, and $q^2 = u^2 + v^2 + w^2$. Given the preconditioning P_0 in Q_0 variables, we can compute the preconditioner P_i in Q_i coordinates by

$$P_i = \frac{\partial Q_i}{\partial Q_0} P_0 \frac{\partial Q_0}{\partial Q_i}, \quad \text{where} \quad \mathrm{P_0} \text{ is given by Eq. (2).}$$

The following transformation matrices connect these variables: Let $\hat{q}^2 = \frac{(\gamma-1)q^2}{2}$

$$\frac{\partial Q_0}{\partial Q_1} = \begin{bmatrix} \hat{q}^2 & (1-\gamma)u & (1-\gamma)v & (1-\gamma)w & \gamma-1 \\ \frac{-u}{\rho} & \frac{1}{\rho} & 0 & 0 & 0 \\ \frac{-v}{\rho} & 0 & \frac{1}{\rho} & 0 & 0 \\ \frac{-w}{\rho} & 0 & 0 & \frac{1}{\rho} & 0 \\ \hat{q}^2 - a^2 & (1-\gamma)u & (1-\gamma)v & (1-\gamma)w & \gamma-1 \end{bmatrix}$$

$$\frac{\partial Q_1}{\partial Q_0} = \begin{bmatrix} \frac{1}{a^2} & 0 & 0 & 0 & \frac{-1}{a^2} \\ \frac{u}{a^2} & \rho & 0 & 0 & \frac{-u}{a^2} \\ \frac{v}{a^2} & 0 & \rho & 0 & \frac{-v}{a^2} \\ \frac{w}{a^2} & 0 & 0 & \rho & \frac{-w}{a^2} \\ \frac{1}{\gamma-1} + \frac{M^2}{2} & \rho u & \rho v & \rho w & \frac{-M^2}{2} \end{bmatrix}$$

$$\frac{\partial Q_0}{\partial Q_4} = \begin{bmatrix} 1 & 0 & 0 & 0 & 0 \\ 0 & 1 & 0 & 0 & 0 \\ 0 & 0 & 1 & 0 & 0 \\ 0 & 0 & 0 & 1 & 0 \\ 1-\gamma & 0 & 0 & 0 & \frac{\gamma p}{T} \end{bmatrix}$$

$$\frac{\partial Q_4}{\partial Q_0} = \begin{bmatrix} 1 & 0 & 0 & 0 & 0 \\ 0 & 1 & 0 & 0 & 0 \\ 0 & 0 & 1 & 0 & 0 \\ 0 & 0 & 0 & 1 & 0 \\ \frac{(\gamma-1)T}{\gamma p} & 0 & 0 & 0 & \frac{T}{\gamma p} \end{bmatrix}$$

To transform the preconditioned residual in (p, u, v, w, T) to and from the conservative variables, we use the following Jacobians, which result directly from those given above:

$$\frac{\partial Q_1}{\partial Q_4} = \begin{bmatrix} \frac{\rho}{p} & 0 & 0 & 0 & \frac{-\rho}{T} \\ \frac{\rho u}{p} & \rho & 0 & 0 & \frac{-\rho u}{T} \\ \frac{\rho v}{p} & 0 & \rho & 0 & \frac{-\rho v}{T} \\ \frac{\rho w}{p} & 0 & 0 & \rho & \frac{-\rho w}{T} \\ \frac{E}{p} & \rho u & \rho v & \rho w & \frac{-\rho q^2}{2T} \end{bmatrix}$$

$$\frac{\partial Q_4}{\partial Q_1} = \begin{bmatrix} \hat{q}^2 & (1-\gamma)u & (1-\gamma)v & (1-\gamma)w & \gamma-1 \\ -\frac{u}{\rho} & \frac{1}{\rho} & 0 & 0 & 0 \\ -\frac{v}{\rho} & 0 & \frac{1}{\rho} & 0 & 0 \\ -\frac{w}{\rho} & 0 & 0 & \frac{1}{\rho} & 0 \\ \frac{(\hat{q}^2-T)}{\rho} & \frac{(1-\gamma)u}{\rho} & \frac{(1-\gamma)v}{\rho} & \frac{(1-\gamma)w}{\rho} & \frac{(\gamma-1)}{\rho} \end{bmatrix}$$

Also, $\Gamma_i = \frac{\partial Q_i}{\partial Q_0} P_0 \frac{\partial Q_0}{\partial Q_c}$, so that $P_i = \Gamma_i \frac{\partial Q_c}{\partial Q_i}$. In particular, $P_c = \frac{\partial Q_1}{\partial Q_4}\Gamma_4$ and $P_4 = \Gamma_4 \frac{\partial Q_1}{\partial Q_4}$. For the

(p, u, v, w, T) variables, we consider only the case in which $\delta = 1$. We define $\hat{T} = \frac{(\gamma-1)T}{\gamma p}$. Then,

$$\Gamma_4 = \begin{bmatrix} \beta^2 & 0 & 0 & 0 & 0 \\ \frac{-u}{\rho}(1+\alpha) & \frac{1}{\rho} & 0 & 0 & 0 \\ \frac{-v}{\rho}(1+\alpha) & 0 & \frac{1}{\rho} & 0 & 0 \\ \frac{-w}{\rho}(1+\alpha) & 0 & 0 & \frac{1}{\rho} & 0 \\ \hat{T}\left[\beta^2 + \frac{q^2}{2} - \frac{a^2}{\gamma-1}\right] & -\hat{T}u & -\hat{T}v & -\hat{T}w & \hat{T} \end{bmatrix}$$

and letting $\hat{E} = \frac{E+p}{\rho} + \alpha q^2$:

$$\Gamma_4^{-1} = \begin{bmatrix} \frac{1}{\beta^2} & 0 & 0 & 0 & 0 \\ \frac{(1+\alpha)u}{\beta^2} & \rho & 0 & 0 & 0 \\ \frac{(1+\alpha)v}{\beta^2} & 0 & \rho & 0 & 0 \\ \frac{(1+\alpha)w}{\beta^2} & 0 & 0 & \rho & 0 \\ \frac{1}{\beta^2}\hat{E} & \rho u & \rho v & \rho w & \frac{\gamma p}{(\gamma-1)T} \end{bmatrix}$$

.

References

[1] Choi, Y.-H. and Merkle, C.L. "*The Application of Preconditioning to Viscous Flows*," Journal of Computational Physics, vol. 105, 1993, pp. 207-223.

[2] Chorin, A.J. "*A Numerical Method for Solving Incompressible Viscous Flow Problems*," Journal of Computational Physics, vol. 2, 1967, pp. 12-26.

[3] Darmofal, D.L. and Schmid, P.J. "*The importance of eigenvectors for local preconditioners of the Euler equations,*" 12th AIAA Computational Fluid Dynamics Conference, 1995, pp.102-117.

[4] Fiterman, A., Turkel, E. and Vatsa, V. "*Pressure Updating Methods for the Steady-State Fluid Equations*," Proceedings 12th AIAA Computational Fluid Dynamics Conference, AIAA Paper 95-1652, 1995.

[5] Jameson, A., Schmidt, W. and Turkel, E. "*Numerical Solutions of the Euler Equations by a Finite Volume Method using Runge-Kutta Time-Stepping Schemes*," AIAA Paper 81-1259, 1981.

[6] Radespiel, R. and Turkel, E. "*Assessment of Preconditioning Methods*," Proceedings of Cerca Conference, 1995.

[7] Radespiel, R., Turkel, E. and Kroll, N. "*Assessment of Preconditioning Methods*," DLR report, 1995.

[8] Swanson, R.C. and Turkel, E. "*Artificial Dissipation and Central Difference Schemes for the Euler and Navier-Stokes Equations*," AIAA Computational Fluid Dynamics Conference, AIAA 87-1107-CP, 1987.

[9] Turkel, E., Fiterman, A. and van Leer, B. "*Preconditioning and the Limit to the Incompressible Flow equations*," Computing the Future: Frontiers of Computational Fluid Dynamics 1994, D.A.Caughey and M.M. Hafez, eds., Wiley Publishing, 1994, pp. 215-234.

[10] Turkel, E. "*Preconditioned Methods for Solving the Incompressible and Low Speed Compressible Equations*," Journal of Computational Physics, vol. 72, 1987, pp. 277-298.

[11] Turkel, E. "*A Review of Preconditioning Methods for Fluid Dynamics*," Applied Numerical Mathematics, vol. 12, 1993, pp. 257-284.

[12] Volpe, G. "*Performance of Compressible Flow Codes at Low Mach Numbers*," AIAA J., vol. 31, 1993, pp. 49-56.

[13] Workshop on High-Lift Flow Physics for Application to Subsonic Aircraft. A workshop held at NASA Langley Research Center, May 18-20, 1993.

[14] Vatsa, V.N., Sanetrik, M.D., Parlette, E.B., Eiseman, P., and Cheng, Z. "Multi-block Structured Grid Approach for Solving Flows over Complex Aerodynamic Configurations," AIAA Paper 94-0655, 1994.

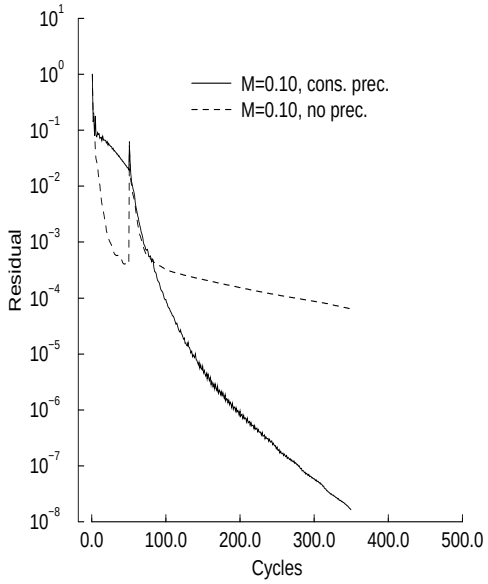

Figure 1: Effect of preconditioning on convergence history for ONERA M6 wing at $M_\infty = 0.10$

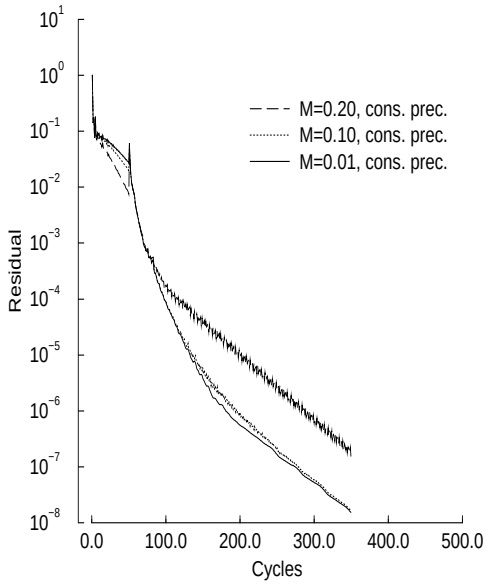

Figure 2: Effect of Mach number on convergence history of the preconditioned scheme for ONERA M6 wing

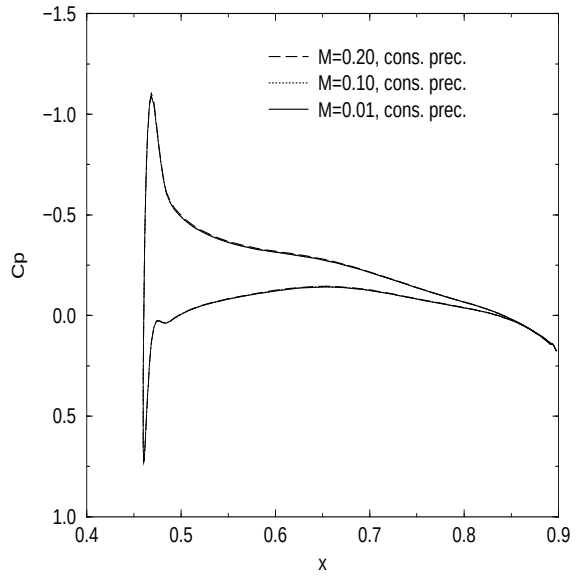

Figure 3: Effect of Mach number on ONERA M6 wing pressure distributions at 80% span location for preconditioned scheme

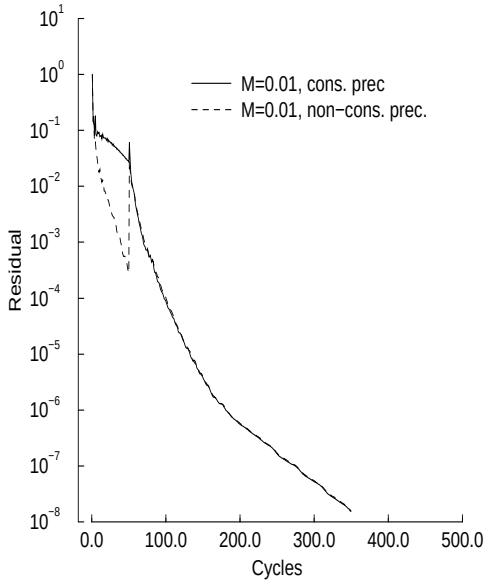

Figure 4: Effect of conservative/non-conservative formulations of artificial dissipation on convergence history for ONERA M6 wing

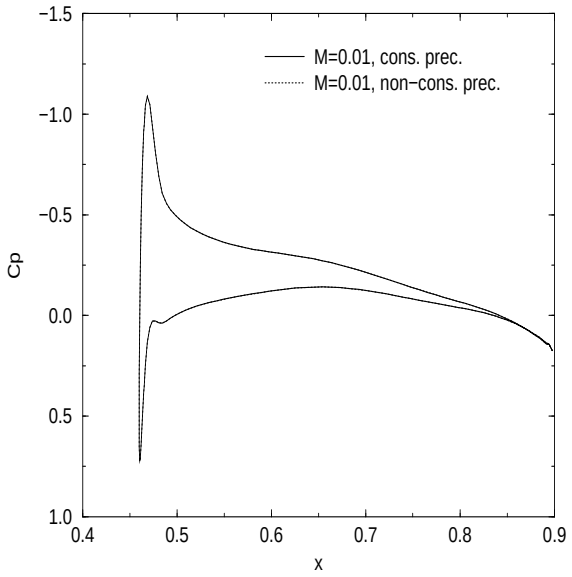

Figure 5: Effect of conservative/non-conservative formulations of artificial dissipation on ONERA M6 wing pressure distributions

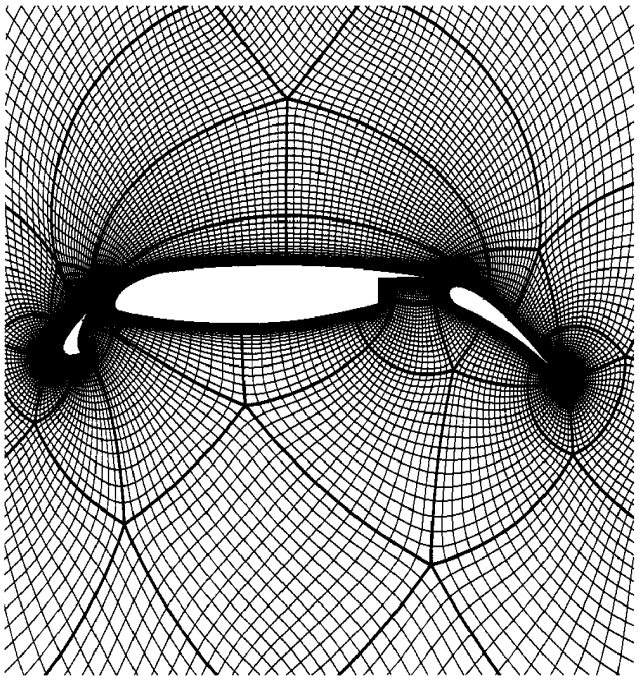

Figure 6: Partial view of block-structured grid for 3-element high lift airfoil configuration

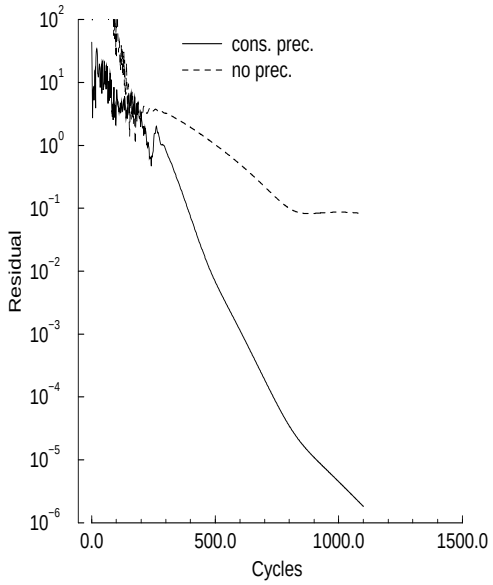

Figure 7: Effect of preconditioning on convergence history for the the 3-element high-lift airfoil configuration

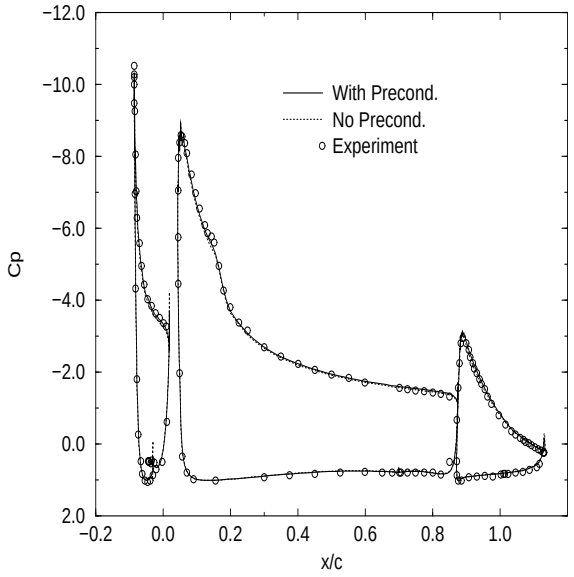

Figure 8: Effect of preconditioning on pressure distributions for the 3-element high-lift airfoil configuration

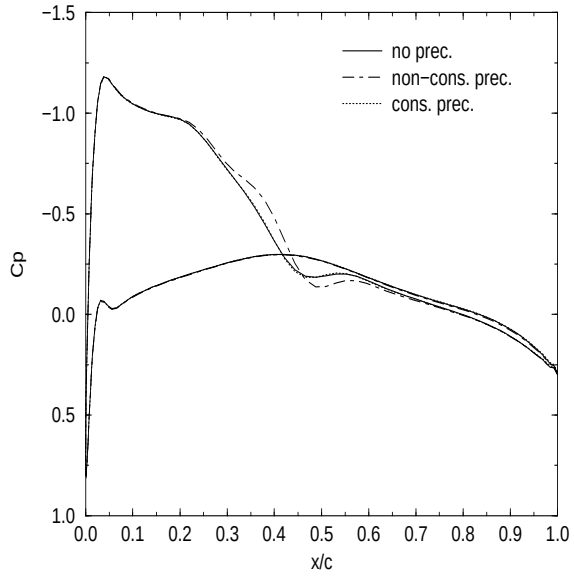

Figure 9: Comparison of pressure distribution for ONERA M6 wing at transonic speeds

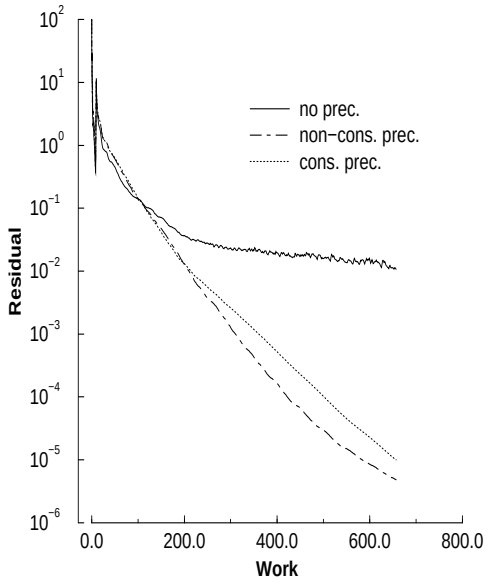

Figure 10: Comparison of convergence histories for ONERA M6 wing at transonic speeds